PHOTONICS Research

Tunable spin splitting of Laguerre–Gaussian beams in graphene metamaterials

Wenguo Zhu,[1,2,4] Mengjiang Jiang,[3,2] Heyuan Guan,[1,5] Jianhui Yu,[2] Huihui Lu,[2] Jun Zhang,[3] and Zhe Chen[3]

[1]*Guangdong Provincial Key Laboratory of Optical Fiber Sensing and Communications, Jinan University, Guangzhou 510632, China*
[2]*Department of Optoelectronic Engineering, Jinan University, Guangzhou 510632, China*
[3]*Key Laboratory of Optoelectronic Information and Sensing Technologies of Guangdong Higher Education Institutes, Jinan University, Guangzhou 510632, China*
[4]*e-mail: zhuwg88@163.com*
[5]*e-mail: ttguanheyuan@jnu.edu.cn*

Received 25 July 2017; revised 19 September 2017; accepted 7 October 2017; posted 9 October 2017 (Doc. ID 302961); published 8 November 2017

Optical spin splitting has attracted significant attention owing to its potential applications in quantum information and precision metrology. However, it is typically small and cannot be controlled efficiently. Here, we enhance the spin splitting by transmitting higher-order Laguerre–Gaussian (LG) beams through graphene metamaterial slabs. The interaction between LG beams and metamaterial results in an orbital-angular-momentum- (OAM) dependent spin splitting. The upper bound of the OAM-dependent spin splitting is found, which varies with the incident OAM and beam waist. Moreover, the spin splitting can be flexibly tuned by modulating the Fermi energy of the graphene sheets. This tunable spin splitting has potential applications in the development of spin-based applications and the manipulation of mid-infrared waves.

OCIS codes: (260.5430) Polarization; (050.4865) Optical vortices; (160.3918) Metamaterials; (310.6628) Subwavelength structures, nanostructures.

https://doi.org/10.1364/PRJ.5.000684

1. INTRODUCTION

Graphene, an atomically thin layer of carbon atoms arranged in a honeycomb lattice, has attracted significant interest owing to its superior electronic and optical properties [1–3]. The conductivity of graphene is very sensitive to external fields, such that its optoelectronic properties can be precisely tuned [4]. Owing to its unique properties, graphene has been suggested as an alternative to conventional metal-based structures to confine light [5], guide surface plasmon polaritons [6], and manipulate wavefronts [7,8]. The subwavelength metamaterial structures made of graphene sheets show advantages over those made of thin metal layers at frequency and amplitude tunable properties [9]. Recently, the graphene metamaterial has been experimentally realized in the mid-infrared range [10]. The metamaterial experiences an optical topological transition from elliptic to hyperbolic dispersion at a wavelength of 4.5 μm [10].

Spin splitting refers to the spatial separation of two opposite spin components of bounded light beams reflected from or transmitted through an interface between two different media [11–14]. The spin splitting phenomenon was first observed experimentally by Hosten and Kwiat in 2008 [11]. In their experiment, a weak measurement was used since the spin splitting of the transmitted beam through an air–glass interface was very small—only a fraction of a wavelength [11,12]. Lately, much larger spin splitting was found by reflected Gaussian beams near Brewster incidence [13]. Götte and coworkers have achieved a spin splitting of ten wavelengths near Brewster incidence by properly choosing the incident polarization state [14]. In 2015, a spin splitting equal nearly to the incident beam waist w_0 was demonstrated when a one-dimensional Gaussian beam with $w_0 = 10.2$ μm was reflected from an air–glass interface [15]. For a two-dimensional Gaussian beam, however, the spin splitting could only reach $0.4w_0$. It was demonstrated that the spin splitting can also be enhanced by metal thin films [16] and metamaterials [17,18]. Recently, the upper bounds of the spin splitting of Gaussian incident beams were found, which were equal to the incident beam waists w_0 [19].

Although less investigated, the beam shifts of higher-order Laguerre–Gaussian (LG) beams are very interesting [20–22]. When reflected by an interface between two different media, the complex vortex structures of LG beams will interact with the angular Goos–Hänchen (GH) and Imbert–Fedorov shifts, which leads to the orbital-angular-momentum- (OAM) dependent shifts along directions both parallel and perpendicular to the plane of incidence [23]. The OAM-dependent shifts increase linearly with the incident OAM, so that large beam shifts can be achieved [24]. These shifts have been used to steer asymmetric spin splitting [25].

Alternatively, here we theoretically show a symmetric spin splitting dependent on the incident OAM when transmitting higher-order LG beams through a graphene metamaterial slab. The metamaterial is based on the multilayer structure of alternating graphene sheets and Al_2O_3 layers. As a result of the interaction between graphene metamaterial and a light beam embedded with OAM, the two opposite spin components of the transmitted beam will undergo shifts toward opposite directions, and the shifts depend on the incident OAM ℓ. The OAM-dependent spin splitting is bounded by $w_0|\ell| \cos\theta_t/[(|\ell|+1)^{1/2}\cos\theta_i]$, where θ_i and θ_t are the incident and transmitted angles, respectively. By modulating the Fermi energy of the graphene sheets, the spin splitting can be tuned from positive to negative. Also, the splitting can reach its upper bound. The Fermi energy of graphene can be tuned over a wide range by an externally applied bias (electrostatic gating) since the Fermi energy in graphene is related to the carrier concentration [26].

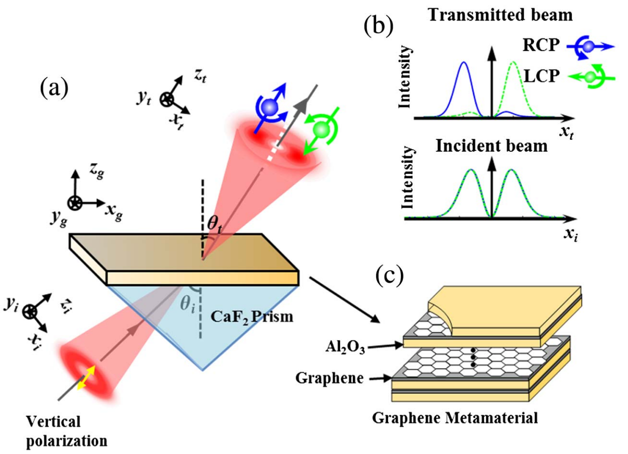

Fig. 1. (a) Schematic of the OAM-dependent spin splitting. A vertically polarized LG beam is coupled into a graphene metamaterial slab through a CaF_2 prism. The two opposite spin components of the transmitted beam will separate along the x_t axis. (b) The intensity distributions of the RCP and LCP components of the incident and transmitted beams along the x_i and x_t axes, respectively. (c) The graphene metamaterial composed of alternating graphene sheets and Al_2O_3 layers.

2. THEORY

The graphene-dielectric multilayer structure can be viewed as a metamaterial with effective medium approximation. In the long-wavelength limit, the effective in-plane and out-of-plane permittivities of the metamaterial respectively are [10]

$$\varepsilon_{\mathrm{eff},//} = \varepsilon_d + i\frac{\sigma Z_0 \lambda}{2\pi d}, \tag{1a}$$

$$\varepsilon_{\mathrm{eff},\perp} = \varepsilon_d, \tag{1b}$$

where ε_d and h are the permittivity and thickness of the dielectric layer, λ is the wavelength in free space, and Z_0 is the vacuum impedance. σ is the optical conductivity of graphene, which is in the form of [1,27]

$$\sigma = \frac{2e^2 k_B T}{\pi\hbar^2}\frac{i}{w + i\tau^{-1}}\ln\left(2\cosh\frac{E_F}{2k_B T}\right) + \frac{e^2}{4\hbar}\left(\frac{1}{2} + \frac{1}{\pi}\tan^{-1}\frac{\hbar w - E_F}{2k_B T}\right) - \frac{i}{2\pi}\ln\frac{(\hbar w + 2E_F)^2}{(\hbar w - 2E_F)^2 + (2k_B T)^2}. \tag{2}$$

Here, k_B is the Boltzmann constant, ω is the frequency of light, E_F is the Fermi energy, $T = 300$ K is the temperature, and τ is the carrier relaxation lifetime. $\tau = \mu E_F/(e v_F^2)$ with $v_F \approx 1\times 10^6$ m/s being the Fermi velocity and $\mu = 10000\ \mathrm{cm}^2\cdot\mathrm{V}^{-1}\cdot\mathrm{s}^{-1}$ being the mobility. As shown by Eq. (1), the real part of the optical conductivity σ raises the absorption of the graphene metamaterial. The image part of σ tunes the real part of the in-plane permittivity of the graphene metamaterial, which can be changed from positive value, zero, to negative value.

In order to investigate the OAM-dependent spin splitting, we launch a linearly polarized higher-order LG beam obliquely onto a graphene metamaterial from a CaF_2 prism, as shown in Fig. 1(a). The incident and transmitted angles are θ_i and θ_t, respectively. The local coordinate systems attached to the incident and transmitted beams are (x_i, y_i, z_i) and (x_t, y_t, z_t), respectively. The angular spectrum of a vertically polarized LG beam is $\tilde{\mathbf{E}}_i = A[w_0(-ik_{ix} + s_\ell k_{iy})/2^{1/2}]^{|\ell|}\exp[-(k_{ix}^2 + k_{iy}^2)w_0^2/4]|V\rangle$, where $A = w_0/(2\pi|\ell|!)^{1/2}$, k_{ix} and k_{iy} are the transverse wave vector of the incident beam, $|V\rangle$ is the vertical polarization state, and $s_\ell = \mathrm{sign}[\ell]$ denotes the sign of the OAM. According to Ref. [12], the angular spectrum of the transmitted beam is connected with that of the incident beam via Fresnel transmission coefficients. In the first order approximation, it is in form of

$$\tilde{\mathbf{E}}_t = \frac{At_s}{k}\left[\frac{w_0(-i\eta k_{tx} + s_\ell k_{ty})}{\sqrt{2}}\right]^{|\ell|}\exp\left[-\frac{(\eta^2 k_{tx}^2 + k_{ty}^2)w_0^2}{4}\right] \times[-\delta_s k_{ty}|H\rangle + (k - i\eta X_s k_{tx})|V\rangle], \tag{3}$$

where $k = 2\pi n/\lambda$ with n being the refractive index of the prism, $k_{tx} = \eta k_{ix}$, $k_{ty} = k_{iy}$, and $\eta = \cos\theta_t/\cos\theta_i$. $X_s = it_s'/t_s$ and $\delta_s = (\eta - t_p/t_s)\cot\theta_i$, with $t_{p,s}$ being Fresnel transmission coefficients for p and s waves and t_s' being the first derivative of t_s. By making an inverse Fourier transformation, we obtain the transmitted light field in real space, which has the following form in circular polarization basis $|\pm\rangle = 2^{-1/2}[|H\rangle \pm i|V\rangle]$:

$$\mathbf{E}_t^{\pm} = \mp it_s\sqrt{\frac{2}{\pi w_0^2|\ell|!}}\exp\left[-\frac{(x_t^2/\eta^2 + y_t^2)}{w_0^2}\right] \times\left\{\left[1 + \frac{X_s x_t/\eta \pm \delta_s y_t}{k w_0^2/2}\right]\left[\frac{(x_t/\eta + is_\ell y_t)}{w_0}\right]^{|\ell|} - \frac{|\ell|[X_s \pm is_\ell\delta_s]}{k w_0}\left[\frac{(x_t/\eta + is_\ell y_t)}{w_0}\right]^{|\ell-1|}\right\}|\pm\rangle. \tag{4}$$

The right- and the left-handed circular polarization (RCP and LCP, respectively) components of the transmitted beam are no longer LG modes. They might lose circular symmetry, thus their centroids might shift, as shown in Fig. 1(b). The displacements of the centroids of the RCP and LCP components of the transmitted beam along the x_t axis are defined as $\Delta_\pm = \iint x_t |E_t^\pm|^2 \mathrm{d}x_t \mathrm{d}y_t / \iint |E_t^\pm|^2 \mathrm{d}x_t \mathrm{d}y_t$ [19]. After some straightforward calculations, we arrive at

$$\Delta_\pm = \frac{\eta[\mathrm{Re}(X_s) \pm \ell \mathrm{Im}(\delta_s)]}{k[1 + (|\ell| + 1)(|X_s|^2 + |\delta_s|^2)/k^2 w_0^2]}. \tag{5}$$

The first term of Eq. (5) is the conventional GH shift originated from the Gaussian envelope [12]. It moves the RCP and LCP components of the transmitted beam together. However, the second term will shift the RCP and LCP components toward opposite directions. The term is OAM dependent, resulting from the coupling between incident OAM and the angular spin splitting $\sigma \mathrm{Im}(\delta_s)$ [28]. This OAM-dependent spin splitting is different from the in-plane photonic spin splitting [29], which vanishes for a vertically incident polarization. The spin splitting of the transmitted beam is defined as the distance between the centroids of two opposite spin components, $\Delta = \Delta_+ - \Delta_-$, which therefore is equal to the OAM-dependent spin splitting, independent from the GH shift. When the second term of the denominator in Eq. (5) is negligible, the spin splitting Δ is linearly proportional to the incident OAM ℓ. Otherwise, the Δ changes nonlinearly with ℓ. To maximize the spin splitting Δ, δ_s should be a pure imaginary number and $|\delta_s| \gg |X_s|$. When $|\delta_s| = kw_0/(|\ell| + 1)^{1/2}$, the maximum Δ is obtained:

$$\Delta_{\mathrm{up}} = \frac{\eta w_0 |\ell|}{\sqrt{|\ell| + 1}}. \tag{6}$$

Therefore, Δ_{up} is the upper bound of the OAM-dependent spin splitting of the transmitted beam, which is determined by the incident OAM, beam waist, and the incident and transmitted angles. It has been already demonstrated that the upper bound of the spin splitting of a reflected Gaussian beam is w_0 [19]. In the transmission case, the upper bound of spin splitting along the x_t axis should be corrected as ηw_0. Therefore, the upper bound of the spin splitting for the Gaussian beam is smaller than those of OAM-dependent spin splitting for LG beams when $|\ell| > 1$. Estimated by the second radial moment of the intensity, the beam size (beam width) of the LG beam is $w_0(|\ell| + 1)^{1/2}$ [30]. For a fixed w_0, the size of the LG beam increases with $|\ell|$. Thus, the ratio between the upper bound of the spin splitting and the beam size of the LG beam is $\eta|\ell|/(|\ell| + 1)$, which shows no advantage over the foundational Gaussian beam. However, the OAM-dependent spin splitting is not only physically interesting [12,22], but it also provides an alternative method for the control of optical spin [25]. As will be shown below, when the OAM-dependent spin splitting reaches its upper bound, the RCP and LCP components of the transmitted LG beam are well separated along the x_t axis: the two intensity profiles RCP and LCP components are distinguishable according to the Rayleigh criterion [15]. However, the profiles are indistinguishable from each other for the case of Gaussian incident beams [19]. In the following, we will try to tune the spin splitting and approximate its upper bound by using graphene metamaterials.

3. RESULTS

Consider the graphene metamaterial composed of alternating Al_2O_3 layers and graphene sheets, with the thickness of Al_2O_3 layers being $h = 10$ nm [see Fig. 1(c)]. The real part of the in-plane permittivity $\mathrm{Re}[\varepsilon_{\mathrm{eff},//}]$ varies with Fermi energy and can take positive, zero, and negative values. When $E_F = 0.335$ eV, $\mathrm{Re}[\varepsilon_{\mathrm{eff},//}]$ almost vanishes for a wavelength of $\lambda = 4.509$ μm. The graphene metamaterial is displaced on the CaF_2 prism, whose reflective index is $n = 1.39$ at $\lambda = 4.509$ μm [10]. The structure can be fabricated by the method provided by Ref. [10].

The spin splitting of the transmitted beam Δ will change with incident angle θ_i and the thickness of metamaterial d, as shown by Fig. 2(a), where Δ is normalized to its upper bound Δ_{up}. In the calculations, the incident OAM is $\ell = 1$, the beam waist is $w_0 = 180$ μm, the Fermi energy of the graphene sheets is $E_F = 0.335$ eV, and the wavelength is $\lambda = 4.509$ μm. In this situation, the effective in-plane permittivity of the graphene metamaterial is $\varepsilon_{\mathrm{eff},//} = -0.001 + 0.086i$. When the incident angle θ_i changes from 10° to 45°, the spin splitting Δ can always approach the upper bound Δ_{up} by modulating d. When $\theta_i = 33°$ and $d = 7.5$ μm, Δ is up to $0.994\Delta_{\mathrm{up}}$. The dependences of normalized spin splitting $\Delta/\Delta_{\mathrm{up}}$ on the incident angle θ_i for $w_0 = 90$ μm (red color), 225 μm (blue color), and 450 μm (green color) are shown respectively in Fig. 2(b), where the thickness of metamaterial is fixed on 7.5 μm. The maximum value of $\Delta/\Delta_{\mathrm{up}}$ changes slightly with the beam waist w_0. For the beam waist ranging from 90 to 450 μm, $\Delta/\Delta_{\mathrm{up}}$ is larger than 0.95, which indicates that Δ is close to its upper bound Δ_{up} over a wide range of w_0.

For the incident beams carried with different values of OAM, the spin splitting of the transmitted beams Δ are different. According to Eq. (6), the upper bounds of the OAM-dependent spin splitting Δ_{up} increases with the OAM $|\ell|$. The change of Δ_{up} with ℓ is shown in Fig. 3(a), where the spin splitting Δ is also shown. Δ is opposite in sign for negative and positive OAM ℓ, and Δ vanishes when $\ell = 0$. Δ and Δ_{up} are identical for the cases of $\ell = \pm 1$ since the parameters $\theta_i = 33°$ and $d =$

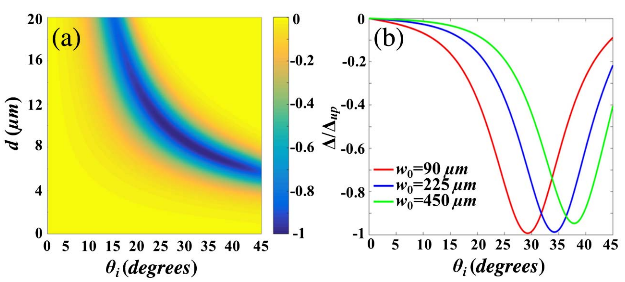

Fig. 2. (a) Changes of the normalized OAM-dependent spin splitting $\Delta/\Delta_{\mathrm{up}}$ with the incident angle θ_i and thickness of metamaterial d when $w_0 = 180$ μm. (b) The dependences of $\Delta/\Delta_{\mathrm{up}}$ on θ_i for $w_0 = 90$ μm (red color), 225 μm (blue color), and 450 μm (green color). In our calculations, $\ell = 1$, $E_F = 0.335$ eV, $d = 7.5$ μm, and $\lambda = 4.509$ μm.

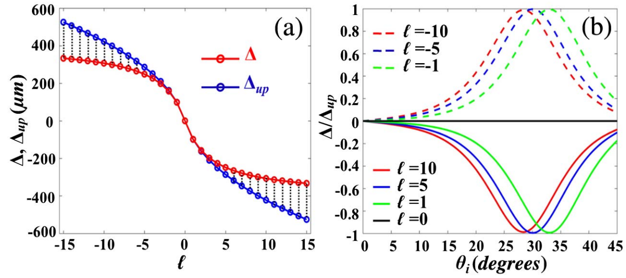

Fig. 3. (a) Changes of the spin splitting Δ (red dots) and its upper bounds $\Delta_{\rm up}$ (blue dots) with the incident OAM ℓ for $\theta_i = 33°$ and $d = 7.5$ μm. (b) The normalized spin splitting $\Delta/\Delta_{\rm up}$ changing with the incident angle θ_i for OAM $\ell = \pm 10$ (red color), ± 5 (blue color), ± 1 (green color), and 0 (black color).

7.5 μm are optimized for these cases, as mentioned above. However, Δ is smaller than $\Delta_{\rm up}$ when $|\ell| > 1$, and the difference increases with $|\ell|$, as shown by Fig. 3(a).

The spin splitting Δ for $|\ell| > 1$ can be increased by slightly changing the incident angle θ_i. Figure 3(b) shows the normalized spin splitting $\Delta/\Delta_{\rm up}$ changing with the incident angle θ_i for OAM $\ell = -10$ (red lines), –5 (blue lines), –1 (green lines), and 0 (black line). For a Gaussian incident beam ($\ell = 0$), the spin splitting vanishes for all the incident angles. However, when $\ell \neq 0$, the spin splitting $|\Delta|$ increases with the incident angle θ_i and decreases gradually after reaching peak. The incident angle of the splitting peak decreases with the increase of $|\ell|$. For all ℓ, the spin splitting can reach more than 0.99 of their upper bounds.

The spin splitting of the transmitted beam can be flexibly tuned by modulating the Fermi energy of the graphene sheets. The normalized spin splitting $\Delta/\Delta_{\rm up}$ changing with Fermi energy E_F for different thicknesses of the graphene metamaterial d are shown in Fig. 4(a), where the incident OAM $\ell = 3$ (solid lines) and $\ell = -3$ (dashed lines). For each situation, there are two peaks in the pattern of the spin splitting: a positive peak and a negative peak. The positive and negative peaks are separated by a zero point, which is located around $E_F = 0.31$ eV. When $d = 7.2$ and 9.0 μm, the spin splitting $|\Delta|$ reach their upper bounds $\Delta_{\rm up}$ at $E_F = 0.336$ and 0.297 eV, respectively. When $d = 8.3$ μm, however, the spin splitting Δ is smaller than $\Delta_{\rm up}$. Interestingly, the absolute values of the spin splitting $|\Delta|$ for positive and negative peaks are identically equal to $0.82\Delta_{\rm up}$. To show the change of the spin splitting with the Fermi energy E_F more clearly, the intensity profiles of the RCP (solid lines) and LCP (dotted lines) components of the transmitted beam along x_t are shown in Fig. 4(b) for $E_F = 0.275$ eV (red color), 0.299 eV (blue color), 0.318 eV (green color), 0.356 eV (pink color), and 0.4 eV (black color) when the thickness of the graphene metamaterial is $d = 8.3$ μm. The intensity profiles of the RCP and LCP components are overlapped when $E_F = 0.318$ eV, indicating the spin splitting $\Delta = 0$. The giant spin splitting is evident in cases of $E_F = 0.299$ and 0.356 eV, where the two opposite spin components are well separated.

The spin splitting will change with the wavelength λ owing to the dispersion of the graphene metamaterial. Figure 5 plots the spin splitting Δ as a function of wavelength λ for different

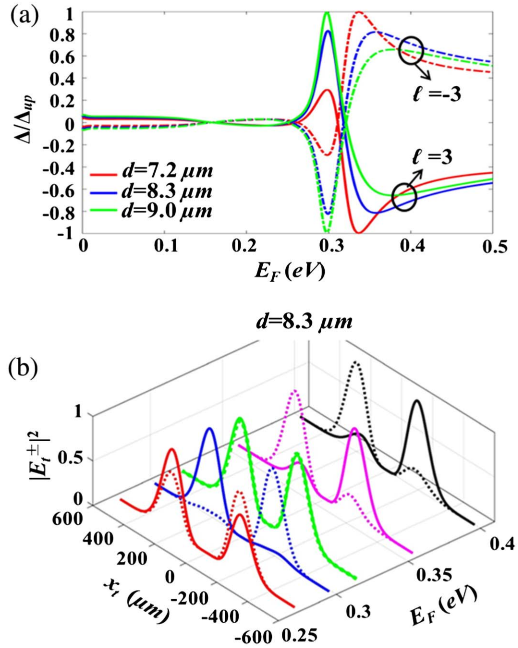

Fig. 4. (a) Dependences of the normalized spin splitting $\Delta/\Delta_{\rm up}$ on the Fermi energy E_F for $\ell = -3$ and $d = 7.2$ μm (red color), 8.3 μm (blue color), and 9.0 μm (green color). (b) The normalized intensities of the RCP (solid lines) and LCP (dotted lines) components of the transmitted beams along the x_t axis for $d = 8.3$ μm and $E_F = 0.275$ eV (red color), 0.299 eV (blue color), 0.318 eV (green color), 0.356 eV (pink color), and 0.4 eV (black color).

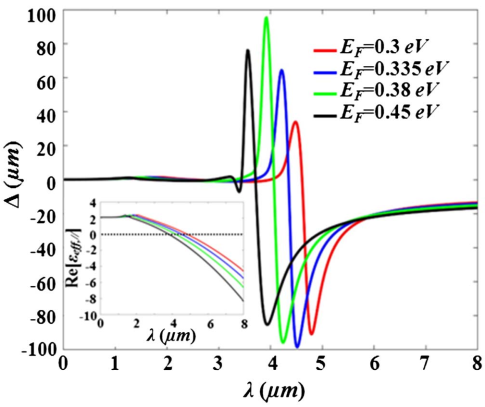

Fig. 5. Spin splitting Δ changing with the wavelength λ when $E_F = 0.3$ eV (red color), 0.335 eV (blue color), 0.38 eV (green color), and 0.45 eV (black color). The inset shows the real part of in-plane permittivity of the graphene metamaterial $\mathrm{Re}[\varepsilon_{\rm eff,//}]$ changing with λ for different values of E_F.

values of Fermi energy E_F. From Fig. 5, one can see that the spin splitting for each E_F almost vanishes in the short wavelength range ($\lambda < 3$ μm). However, Δ will increase suddenly and reach peak value. After that, it decreases sharply until reaching a negative peak. Then it will increase gradually. It is worth noticing that the magnitudes of the positive and negative peaks are different. The spin splitting undergoes blueshift when the Fermi energy E_F increases. This phenomenon can be explained by the move of the zero points of the real part of the in-plane permittivity, $\mathrm{Re}[\varepsilon_{\mathrm{eff},//}]$, as shown in the inset of Fig. 5, where the changing of $\mathrm{Re}[\varepsilon_{\mathrm{eff},//}]$ with wavelength λ for different values of Fermi energy E_F are shown.

From Fig. 5, one can conclude that the giant spin splitting is associated with the near-zero $\mathrm{Re}[\varepsilon_{\mathrm{eff},//}]$. In these cases, however, the image part of the in-plane permittivity, $\mathrm{Im}[\varepsilon_{\mathrm{eff},//}]$, is nonzero, which causes loss. Specially, at the upper-bounded spin splitting, the energy transmissivity is of the order of 10^{-5}. It is worth pointing out that the energy transmissivity is of the same order of magnitude when a reflected Gaussian beam reaches its upper-bounded spin splitting at Brewster incidence [19], and this upper-bounded spin splitting has been experimentally measured [29]. Therefore, the low-energy transmissivity will not prevent the experimental measurement of giant spin splitting of the transmitted beam through graphene metamaterial.

4. CONCLUSION

We have theoretically demonstrated the tunable OAM-dependent spin splitting by transmitting higher-order LG beams through graphene metamaterials. The upper bound of the OAM-dependent spin splitting is $\eta w_0|\ell|/[(|\ell|+1)^{1/2}]$, which increases with the incident OAM $|\ell|$. The Fermi energy of the graphene sheets can change the effective permittivity of the graphene metamaterial, which therefore tune the spin splitting. The spin splitting can be tuned from positive to negative values and can reach its upper bound. These findings provide an effective method for the flexible control of the spin splitting and therefore facilitate the development of spin-based applications and the manipulation of the mid-infrared waves.

Funding. National Natural Science Foundation of China (NSFC) (61505069, 61675092, 61705086); Guangzhou Science and Technology Program key projects (2017A010102006, 2017A030313375).

REFERENCES

1. F. H. L. Koppens, D. E. Chang, and F. J. García De Abajo, "Graphene plasmonics: a platform for strong light-matter interactions," Nano Lett. **11**, 3370–3377 (2011).
2. J.-M. Poumirol, P. Q. Liu, T. M. Slipchenko, A. Y. Nikitin, L. Martin-Moreno, J. Faist, and A. B. Kuzmenko, "Electrically controlled terahertz magneto-optical phenomena in continuous and patterned graphene," Nat. Commun. **8**, 14626 (2017).
3. S. Dai, Q. Ma, M. K. Liu, T. Andersen, Z. Fei, M. D. Goldflam, M. Wagner, K. Watanabe, T. Taniguchi, M. Thiemens, F. Keilmann, G. C. A. M. Janssen, S.-E. Zhu, P. Jarillo-Herrero, M. M. Fogler, and D. N. Basov, "Graphene on hexagonal boron nitride as a tunable hyperbolic metamaterial," Nat. Nanotechnol. **10**, 682–686 (2015).
4. T. Q. Tran, S. Lee, H. Heo, and S. Kim, "Tunable wide-angle tunneling in graphene-assisted frustrated total internal reflection," Sci. Rep. **6**, 19975 (2016).
5. A. Woessner, M. B. Lundeberg, Y. Gao, A. Principi, P. Alonso-González, M. Carrega, K. Watanabe, T. Taniguchi, G. Vignale, M. Polini, J. Hone, R. Hillenbrand, and F. H. L. Koppens, "Highly confined low-loss plasmons in graphene-boron nitride heterostructures," Nat. Mater. **14**, 421–425 (2014).
6. D. Smirnova, S. H. Mousavi, Z. Wang, Y. S. Kivshar, and A. B. Khanikaev, "Trapping and guiding surface plasmons in curved graphene landscapes," ACS Photon. **3**, 875–880 (2016).
7. H. Cheng, S. Chen, P. Yu, W. Liu, Z. Li, J. Li, B. Xie, and J. Tian, "Dynamically tunable broadband infrared anomalous refraction based on graphene metasurfaces," Adv. Opt. Mater. **3**, 1744–1749 (2015).
8. N. Mohammadi Estakhri and A. Alù, "Wave-front transformation with gradient metasurfaces," Phys. Rev. X **6**, 41008 (2016).
9. X. He, P. Gao, and W. Shi, "A further comparison of graphene and thin metal layers for plasmonics," Nanoscale **8**, 10388–10397 (2016).
10. Y. Chang, C. Liu, C. Liu, S. Zhang, and S. R. Marder, "Realization of mid-infrared graphene hyperbolic metamaterials," Nat. Commun. **7**, 10568 (2016).
11. O. Hosten and P. Kwiat, "Observation of the spin hall effect of light via weak measurements," Science **319**, 787–790 (2008).
12. K. Y. Bliokh and A. Aiello, "Goos–Hänchen and Imbert–Fedorov beam shifts: an overview," J. Opt. **15**, 14001 (2013).
13. H. Luo, X. Zhou, W. Shu, S. Wen, and D. Fan, "Enhanced and switchable spin Hall effect of light near the Brewster angle on reflection," Phys. Rev. A **84**, 43806 (2011).
14. J. B. Götte, W. Löffler, and M. R. Dennis, "Eigenpolarizations for giant transverse optical beam shifts," Phys. Rev. Lett. **112**, 233901 (2014).
15. J. L. Ren, B. Wang, Y. F. Xiao, Q. Gong, and Y. Li, "Direct observation of a resolvable spin separation in the spin Hall effect of light at an air–glass interface," Appl. Phys. Lett. **107**, 111105 (2015).
16. X. Tan and X. Zhu, "Enhancing photonic spin Hall effect via long-range surface plasmon resonance," Opt. Lett. **41**, 2478–2481 (2016).
17. T. Tang, C. Li, and L. Luo, "Enhanced spin Hall effect of tunneling light in hyperbolic metamaterial waveguide," Sci. Rep. **6**, 30762 (2016).
18. W. Zhu and W. She, "Enhanced spin Hall effect of transmitted light through a thin epsilon-near-zero slab," Opt. Lett. **40**, 2961–2964 (2015).
19. W. Zhu, J. Yu, H. Guan, H. Lu, J. Tang, J. Zhang, Y. Luo, and Z. Chen, "The upper limit of the in-plane spin splitting of Gaussian beam reflected from a glass–air interface," Sci. Rep. **7**, 1150 (2017).
20. K. Y. Bliokh, I. V. Shadrivov, and Y. S. Kivshar, "Goos–Hänchen and Imbert–Fedorov shifts of polarized vortex beams," Opt. Lett. **34**, 389–391 (2009).
21. M. Merano, N. Hermosa, J. P. Woerdman, and A. Aiello, "How orbital angular momentum affects beam shifts in optical reflection," Phys. Rev. A **82**, 023817 (2010).
22. A. Aiello, "Goos–Hänchen and Imbert–Fedorov shifts: a novel perspective," New J. Phys. **14**, 013058 (2012).
23. Z. Xiao, H. Luo, and S. Wen, "Goos–Hänchen and Imbert–Fedorov shifts of vortex beams at air left-handed-material interfaces," Phys. Rev. A **85**, 33–35 (2012).
24. X. Wang, H. Wang, and F. Zheng, "Properties of group delay for photon tunneling through dispersive metamaterial barriers," Opt. Commun. **382**, 371–376 (2017).
25. J. Zhang, Z. Luo, H. Luo, and S. Wen, "Steering asymmetric spin splitting in photonic spin Hall effect by orbital angular momentum," Acta Opt. Sin. **33**, 1126002 (2013).
26. X. Liu, Z. Chen, E. P. J. Parrott, B. S.-Y. Ung, J. Xu, and E. Pickwell-MacPherson, "Graphene based terahertz light modulator in total internal reflection geometry," Adv. Opt. Mater. **3**, 1600697 (2016).
27. J. Zhang, W. Liu, Z. Zhu, X. Yuan, and S. Qin, "Towards nano-optical tweezers with graphene plasmons: Numerical investigation of trapping 10-nm particles with mid-infrared light," Sci. Rep. **6**, 38086 (2016).
28. W. Zhu, J. Yu, H. Guan, H. Lu, J. Tang, Y. Luo, and Z. Chen, "Large spatial and angular spin splitting in a thin anisotropic ε-near-zero metamaterial," Opt. Express **25**, 5196–5205 (2017).
29. X. Qiu, Z. Zhang, L. Xie, J. Qiu, F. Gao, and J. Du, "Incident-polarization-sensitive and large in-plane-photonic-spin-splitting at the Brewster angle," Opt. Lett. **40**, 1018–1021 (2015).
30. C. Paterson, "Atmospheric turbulence and orbital angular momentum of single photons for optical communication," Phys. Rev. Lett. **94**, 153901 (2005).